Physics-based approach for predicting dissolution?diffusion tool wear in machining

CIRP Annals - Manufacturing Technology 00 (2020) 1–4

Contents lists available at ScienceDirect

CIRP Annals - Manufacturing Technology

journal homepage: https://www.editorialmanager.com/CIRP/default.aspx

Physics-based approach for predicting dissolution–diffusion tool wear in machining

Amir Malakizadi[a,b,*], Bin Shi[c], Philipp Hoier[a], Helmi Attia (1)[c,d], Peter Krajnik (2)[a]

[a] Department of Industrial and Materials Science, Chalmers University of Technology, Gothenburg, Sweden
[b] Department of Modelling and Simulation, AB Sandvik Coromant, Sandviken, Sweden
[c] Aerospace Manufacturing Technology Centre, National Research Council Canada, Montreal, QC, Canada
[d] Department of Mechanical Engineering, McGill University, Montreal, QC, Canada

ARTICLE INFO

Article history:
Available online xxx

Keywords:
Cutting
wear
modelling

ABSTRACT

A new approach is proposed to predict the thermally-activated dissolution-diffusion wear of carbide tools. Departing from the iterative procedure used for such nonlinear processes, a direct response surface approach that correlates the cutting conditions and wear level to the interface temperature is presented. For prediction of wear evolution, a calibrated thermodynamic model that describes chemical interaction between the tool and workpiece materials is combined with the FE simulation of machining process, considering the pressure-dependent thermal constriction resistance phenomenon. The accuracy of predicting flank wear in turning C50 plain carbon steel – where dissolution-diffusion wear mechanism prevails – is validated experimentally.

1. Introduction

Excessive tool wear impairs the dimensional accuracy and the machined surface integrity, for example, by generating tensile surface residual stresses. The cutting parameters optimization for timely tool change scheduling, to minimize the scrap rate, depends on the accurate estimation of tool wear during cutting. Early investigations focused primarily on derivation of empirical tool life equations. In the last decades, several attempts were made to develop phenomenological [1] and physics-based [2] models to predict the tool wear. These efforts aimed at reducing the machining experiments needed to calibrate the models, without a significant compromise on accuracy. The phenomenological models relate the tool wear rate to the tribological parameters, e.g. the temperature, sliding velocity and pressure on the tool surfaces [3]. The physics-based models attempt to estimate the wear rate in terms of the underlying mechanisms e.g. combined effects of abrasion-dissolution [2] or adhesion-diffusion mechanisms [4]. These models include the effects of variations within the workpiece material, e.g. types and amounts of micro-constituents, and the physico-chemical properties of the tool material.

Kramer and Suh [5] have developed a model to predict the thermally-activated dissolution-diffusion wear process, which is primarily observed when uncoated cemented carbides are used in high speed machining of non-ferrous and ferrous metals. The application of this model requires the real-time measurement of the tool-chip interface temperature using the tool-workpiece dynamic thermocouple, which suffers from a number of measurement uncertainties. This model has other limitations that can result in a significant error in estimating the solubility of the tool materials (e.g. WC) in iron, which relies on the temperature-independent 'excess free energies' determined from phase equilibriums at certain temperatures [5]. This shortcoming is also encountered in Gimenez's estimations [6]. Thus, the aim of this work is to propose a new approach to predict dissolution-diffusion wear of carbide tools that overcomes the mentioned limitations, and can readily be adaptable to include different alloying elements in steel, unlike the original approach of Kramer and Suh [5].

2. Materials and machining tests

Orthogonal cutting tests were conducted under dry condition, at five different cutting speeds (v_C) in the range of 100 to 300 m/min. The feed rate and depth of cut were kept constant at 0.1 mm/rev and 2 mm, respectively. Uncoated carbide tools

(WC-10% Co) with 0° rake and 7° clearance angles, and edge radius (r) of 20 ± 2 μm were used. The tests were stopped at 30 m of spiral cutting length to ensure the same contact length between the tool and workpiece for all cases. The workpiece material was C50 steel in as-received condition (63 vol.% pearlite and 166 kg/mm^2 Vickers hardness). The selection of tool-workpiece materials and the range of cutting conditions ensured that the dissolution-diffusion wear mechanism prevails.

3. Tool wear by dissolution – diffusion

Investigations using advanced surface analysis techniques showed that the tungsten carbide and cobalt in the uncoated tools transfer into the chip [7], leading to wear development on the edge. The rate of the mass-transfer depends on the interface temperature and the chemical affinity of the tool and workpiece materials. Kramer and Suh [5] associated the rate of the thermally-activated wear with the

* Corresponding author.
E-mail address: amir.malakizadi@chalmers.se (A. Malakizadi).

https://doi.org/10.1016/j.cirp.2020.04.040

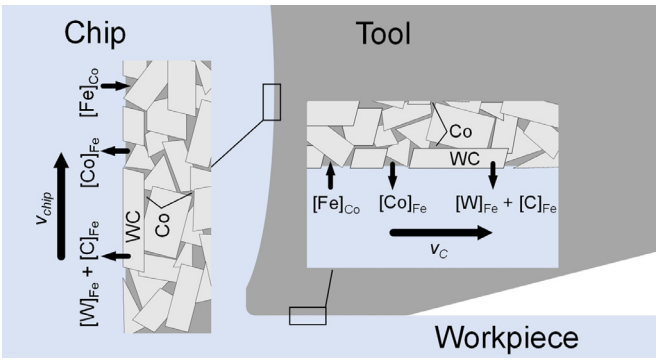

Fig. 1. Thermally-activated wear mechanism: the mass-transfer due to dissolution leads to wear of WC—Co tools when machining steels.

chemical solubility of the tool materials into the workpiece. When uncoated WC—Co tools are used to cut iron-base materials, WC dissociates into W and C at the tool-chip-workpiece interfaces and dissolves into the iron (see Fig. 1 for possible scenarios). The WC can also dissolve into the surrounding Co binder and transfer into the chip-workpiece, as the Co dissolves at the interfaces. This effect is disregarded in this investigation.

If the equilibrium condition holds at the interface, the reaction for the dissolution of WC in iron can be described as:

$$WC \Leftrightarrow [W]_{Fe} + [C]_{Fe} \quad (1)$$

where, $[W]_{Fe}$ and $[C]_{Fe}$ represent the tungsten and carbon dissolved in iron, respectively. A similar phenomenon can occur on both rake and flank surfaces, however the rate of mass transfer on the flank surface would be slower due to lower interface temperature. The dominance of the dissolution-diffusion mechanism on the flank wear surface can be perceived from the characterization results presented in Fig. 2. The topographies of the flank and crater wear surfaces, at v_C = 300 m/min, and their respective local misorientation maps, obtained using Scanning Electron Microscopy and Electron Backscatter Diffraction technique, indicate a limited surface deformation of tungsten carbide grains on both flank and rake surfaces. Hoier et al. [8] associated this small surface deformation with the dominance of thermally-activated wear mechanisms when machining 316 L austenitic stainless steel using uncoated tools, at cutting speeds as low as 120 m/min. In cases where abrasion mechanism is dominant, larger surface deformation is observed on tungsten carbide grains.

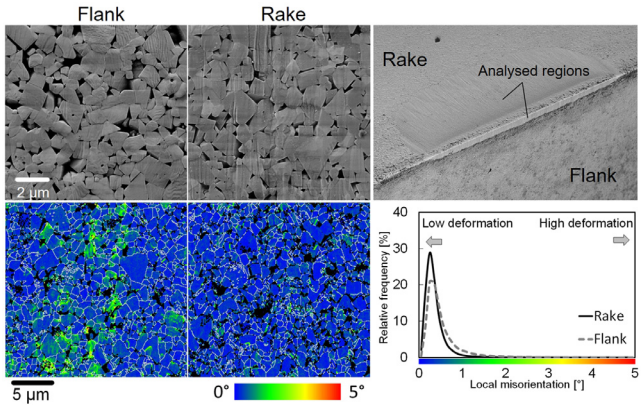

Fig. 2. The topography of the flank and crater wear surfaces and the local misorientation maps of respective surfaces.

3.1. Thermodynamic estimation of solubility of WC in iron

The change in Gibbs free energy due to dissolution of WC in iron is zero at the equilibrium:

$$\Delta G_D = \Delta\overline{G}_W^M + \Delta\overline{G}_C^M - \Delta G_F = 0 \quad (2)$$

where, ΔG_F is the Gibbs free energy of formation for WC, and $\Delta\overline{G}_W^M$ and $\Delta\overline{G}_C^M$ are the partial molar free energies of solution of tungsten and carbon in iron, respectively, which can be expressed as: $\Delta\overline{G}_W^M = RT\ln(a_W)$ and $\Delta\overline{G}_C^M = RT\ln(a_C)$ [5]. Here, a_W and a_C are the activity of tungsten and carbon in iron, respectively, and R is the universal gas constant (R = 8.314 J/mol K). Hence, the change in Gibbs free energy due to dissolution can be given by:

$$\Delta G_D = RT\ln(a_W.a_C) - \Delta G_F = 0 \quad (3)$$

The solubility of WC in iron can thus be obtained for a given temperature by solving Eq. (3). The Gibbs free energy for dissolution of WC in α-iron (ferrite: BCC phase) and γ-iron (austenite: FCC phase) can be described using a two sub-lattice model. In this model, tungsten and iron belong to the substitutional (metal) sub-lattice, whereas carbon and vacancies occupy the interstitial sub-lattice: $(Fe, W)_n(C, Va)_m$, where n and m are the number of sites on each sub-lattice [9]. Following this definition, the Gibbs free energy of solution (G^M) can be formulated as a function of temperature and the concentration of iron, tungsten and carbon in the solution. The complete description of the energy formulation can be found in [9]. The partial molar energies, and thus the activity of carbon and tungsten, can be obtained using the following relations [10]:

$$\Delta\overline{G}_W^M = RT\ln(a_W) = (1-y_W)\left(\frac{\partial G^M}{\partial y_W} - \frac{\partial G^M}{\partial y_{Fe}}\right) + (G^M - G_W^0) \quad (4)$$

$$\Delta\overline{G}_C^M = RT\ln(a_C) = \frac{1}{m}\left(\frac{\partial G^M}{\partial y_C} - \frac{\partial G^M}{\partial y_{Va}}\right) - G_C^0 \quad (5)$$

where, y_W, y_{Fe}, y_C and y_{Va} are the site fractions of tungsten, iron, carbon and vacancy in respective sub-lattices and G_W^0 and G_C^0 are the Gibbs energies of pure tungsten and carbon (graphite). In Eq. (5), m = 3 for α-iron and $m = 1$ for γ-iron, and $y_W = 1 - y_{Fe} = X_W$ and $y_C = 1 - y_{Va} = X_C/(m - mX_C)$, where X_W and X_C are the mole fractions of tungsten and carbon. Using the proper sets of parameters for the C-Fe-W [9] and Fe-C [11] systems, the activity of carbon and tungsten can be calculated at given temperature and concentration. Fig. 3 shows the calculated activity of carbon in α-iron and γ-iron, using Eq. (5) at different temperatures and carbon concentrations, and experimentally reported values [11]. The figure also shows the calculated activity of tungsten using Eq. (4), and its comparison with experimental measurements at two temperatures [9]. A good agreement between the experimental and calculated activities was achieved.

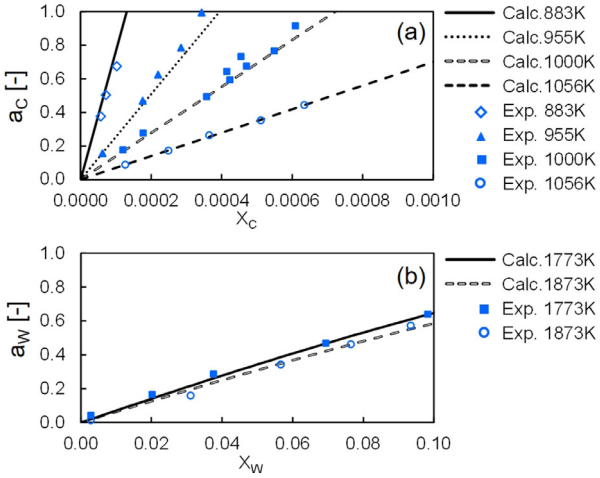

Fig. 3. Calculated and measured [9,11] activities of (a) carbon and (b) tungsten in α-iron at different temperatures and solute concentrations.

Once Eq. (3) is satisfied, the equilibrium concentration of W and C, and thus the amount of WC dissolved in iron (in mole), can be obtained at given temperatures, i.e. the solubility of WC in iron given as $S_{WC} = X_W/(1 - X_W)$. Here, the secant iterative method was implemented in MATLAB® programme to determine the solubility of WC in iron at different temperatures provided that $X_W = X_C$. This approach is referred to as *Method I* in Fig. 4.

Please cite this article as: A. Malakizadi et al., Physics-based approach for predicting dissolution–diffusion tool wear in machining, CIRP Annals - Manufacturing Technology (2020), https://doi.org/10.1016/j.cirp.2020.04.040

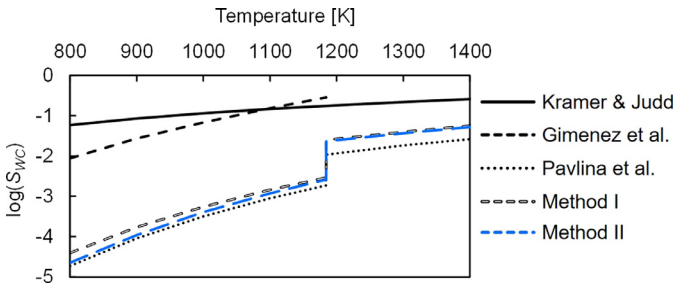

Fig. 4. The calculated solubility of WC in iron (S_{WC}) and the comparisons with other estimations in literature [6, 12, 13].

The Gibbs free energy of dissolution given in Eq. (3) can also be simplified for the composition ranges where the Henrian behaviour is observed [5]. This is generally the case for dilute solutions. The activity of the component i for dilute solutions can be given as $a_i = \gamma_i X_i$ where γ_i is the activity coefficient and X_i is the mole fraction of compound i in the solution. Hence, the mole fraction of tungsten and carbon in solution can be obtained using the following formula:

$$X_W = X_C = \exp\left(\frac{\Delta G_F - RT\ \ln(\gamma_W) - RT\ln(\gamma_C)}{2RT}\right) \tag{6}$$

This relation is equivalent to the equation proposed by Kramer and Judd [12], considering that the relative partial molar excess free energy of solution of component i is given as $\overline{G}_i^{xs} = RT\ln(\gamma_i)$. The mole fraction of solute atoms can thus be determined, if the activity coefficients are known. The solubility of WC is calculated using the activity coefficients obtained by Thermo-Calc® software. This approach is referred to as *Method II*.

Fig. 4 presents the equilibrium concentration of the solute atoms (i.e. the solubility of WC in iron) obtained using *Method I* and *II* at different temperatures and their comparison with the estimations by Pavlina et al. [13], Kramer and Judd [12] and Gimenez et al. [6]. Evidently, the two latter studies overestimate the solubility of WC by several orders of magnitude, due to the imprecise way of estimating the $\overline{G}_W^{xs}$ and $\overline{G}_C^{xs}$. Fig. 3 shows clearly that $\overline{G}_C^{xs}$ is indeed extremely sensitive to temperature. Thus, an accurate estimation of solubility of WC is possible only if the temperature-dependent $\overline{G}_C^{xs}$ and $\overline{G}_W^{xs}$ are used for the calculations.

3.2. Derivation of the wear model

The volume of material that dissolves into the workpiece results in evolution of wear on the tool flank (VB) during machining. The volume of the material removed from the tool edge (ΔV) during a time interval ($\Delta t = t_{n+1} - t_n$) is related to the changes in the width of the flank wear within that time interval ($\Delta VB = VB_{n+1} - VB_n$):

$$\Delta V = a_p \int_{VB_n}^{VB_{n+1}} g(VB, \alpha, r)\, dVB \tag{7}$$

where a_p is the depth of cut and the function $g = dA/dVB$ accounts for the changes in area of the tool cross-section with flank wear evolution, α is the clearance angle and r is the edge radius. The change in flank wear width can thus be obtained during the time interval Δt as:

$$\Delta V - KM_{WC}S_{WC}[T(VB_{n+1}, v_S)]v_S\Delta t = 0 \tag{8}$$

where K is the only constant to be determined using experimental wear measurements, M_{WC} is the molar volume of the tungsten carbide as the main constituent of the tool (in mm^3/mole), S_{WC} is the calculated solubility of WC (in mole) at the interface temperature T, which varies with sliding velocity (v_S) and the width of flank wear (VB) as it evolves. The sliding velocity on the flank surface of the tool is assumed to be equal to the cutting speed i.e. $v_S = v_C$.

4. Finite element modelling and tool wear prediction

Replacing the measurement of the average contact temperature T during machining by calculations based on the computationally intensive FE simulation of the cutting process is not feasible for real time applications. This is further complicated by the nonlinear nature of the problem, in which T is both affecting and being affected by the tool wear (VB) at the same time. Additionally, for accurate prediction of T, the thermal constriction phenomenon at the contact interface has to be considered [14] and formulated as a function of the contact pressure and the contact temperature (which is a source of material nonlinearity). Hence, a new approach is adopted in this investigation to deal with various sources of nonlinearities associated with the tool wear predictions.

Following the approach described in [3], FE models were initially developed based on 15 different combinations of flank wear width (varying between 0–0.3 mm) and cutting speed (varying between 100–300 m/min). The tool was considered as a rigid object, while the workpiece material was assumed to be elasto-viscoplastic, and described by the flow stress model proposed by Childs [15] for carbon steels:

$$\sigma(\varepsilon, \dot{\varepsilon}, T) = H(\varepsilon)(1+\dot{\varepsilon})^{\vartheta}\left(1 - 0.00091T + 1.56 \times 10^{-7}T^2 + 0.25\exp\left(-6.5 \times 10^{-5}(T-650)^2\right)\right) \tag{9}$$

where $\vartheta = 0.035 + 1.2 \times 10^{-4}(T-600)$ for $T > 600°C$, and

$$H(\varepsilon) = \begin{cases} 480(1+\varepsilon/0.0055)^{0.15} & \varepsilon \le 1 \\ 480(1+1/0.0055)^{0.15} & \varepsilon > 1 \end{cases} \tag{10}$$

The thermal softening parameters in Eq. (9) were taken directly from [15]. The parameters of the strain hardening and strain rate hardening terms in Eq. (9) and Eq. (10) were re-evaluated for C50 using an inverse approach described in [16]. Note here that H is given in MPa. The friction condition at the tool-chip-workpiece interfaces was simulated using a pressure dependent shear friction model given in [16]. The heat-transfer coefficient between the tool and chip (and workpiece) was estimated, taking into consideration the thermal constriction phenomenon [17], which is both contact pressure and temperature dependent. The elastic and thermal properties for C50 plain carbon steel were obtained using JMatPro® software. The thermal properties of the tool are given in [16]. Both friction and heat-transfer models were implemented in DEFORM 2D using Fortran subroutines. Fig. 5 summarises the simulated results and their comparison with the measurements. The maximum temperatures shown in Fig. 5(a) at 100 and 200 m/min agree well with the experimental measurements reported in [18]. The nodal temperature on the flank wear land was then extracted from the FE models at 10 different time-steps between 3.5 and 4 mm of cut and the average

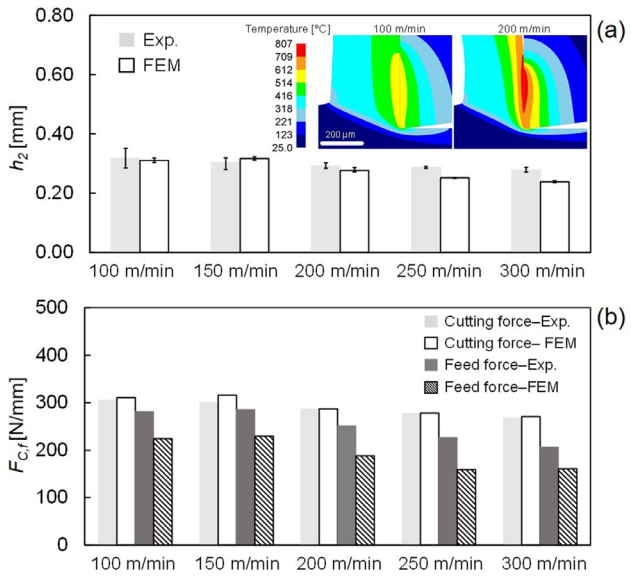

Fig. 5. (a) The simulated chip thickness (h_2) and (b) cutting and feed forces (F_C and F_f) at different cutting speeds (v_C).

Please cite this article as: A. Malakizadi et al., Physics-based approach for predicting dissolution–diffusion tool wear in machining, CIRP Annals - Manufacturing Technology (2020), https://doi.org/10.1016/j.cirp.2020.04.040

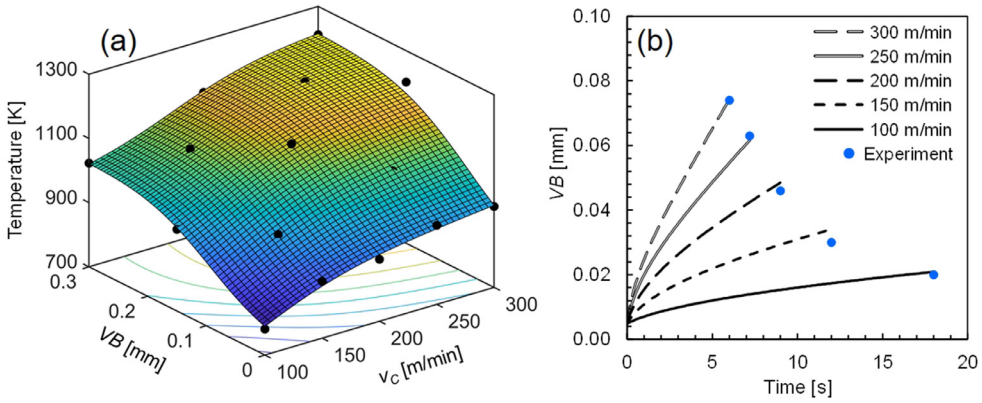

Fig. 6. (a) The average interface temperature as a function of flank wear width and cutting speed and (b) the wear model predictions.

temperatures were calculated for each case. The response surface which relates the average interface temperature T on the wear land and the DoE parameters i.e. VB and v_S was determined using the Artificial Neural Network (ANN) toolbox in MATLAB®. A network with two hidden layers was trained using the Bayesian Regularisation algorithm to obtain an accurate temperature model. The result of the trained network is shown in Fig. 6(a). The black dots show the FE simulation results used as input. Once the temperature function, $T(VB_n, v_S)$, and thus the solubility of WC in iron, $S_{WC}(T)$, are known, the wear model given by Eq. (8) can be calibrated using the wear measurements. Here, the model was calibrated using the flank wear width obtained at 300 m/min (T<1184 K), and it can be written as:

$$\Delta V - 2.85 \times 10^{-3}\left(10^{10.93\log(T(VB_{n+1},v_S))-36.1}\right)v_S\Delta t = 0 \qquad (11)$$

where the geometrical volume loss, ΔV, at time interval Δt is calculated using Eq. (7) and the solubility of WC in iron (S_{WC}) was calculated using *Method I* described in Section 3.1, VB is in mm, v_S is in mm/s, T is in Kelvin and Δt was assumed 0.1 s. Fig. 6(b) shows a good agreement between the calibrated wear model predictions and the experimental data.

5. Conclusions

The novel thermodynamic model presented in this study allows for an accurate prediction of dissolution-diffusion induced tool wear in machining. This approach is readily adaptable for any arbitrary combination of tool-workpiece materials to include the effects of the alloying elements on the solubility of tool materials in highly alloyed workpiece materials, like austenitic stainless steels. The developed physics-based wear model requires only one parameter to be calibrated experimentally, hence it significantly reduces the costly experimental efforts needed for machinability assessment of a given tool-workpiece material combination in terms of tool life. A robust and accurate prediction of tool interface temperature by combining FE modelling, design of experiment and ANN allowed for an efficient modelling of the nonlinear wear process compared to the previous methods reported in the literature which rely on costly iterative FE simulations.

Acknowledgements

This research was supported by Chalmers Area of Advance- Production. The collaboration between Chalmers Centre for Metal Cutting Research (MCR) and NRC's Aerospace Manufacturing Technology Centre (AMTC) is gratefully acknowledged.

References

[1] Usui E, Shirakashi T, Kitagawa T (1984) Analytical Prediction of Cutting Tool Wear. *Wear* 100(1–3):129–151.
[2] Kramer BM, von Turkovich BF (1986) A Comprehensive Tool Wear Model. *CIRP Annals* 35(1):67–70.
[3] Malakizadi A, Gruber H, Sadik I, Nyborg L (2016) An FEM-based Approach for Tool Wear Estimation in Machining. *Wear* 368–369:10–24.
[4] Kannatey A (1985) A Transport-Diffusion Equation in Metal Cutting and its Application to Analysis of the Rate of Flank Wear. *Journal of Engineering for Industry* 107(1):81–89.
[5] Kramer BM, Suh NP (1980) Tool Wear by Solution: A Quantitative Understanding. *Journal of Engineering for Industry* 102(4):303–309.
[6] Giménez S, Van der Biest O, Vleugels J (2007) The Role of Chemical Wear in Machining Iron Based Materials by PCD and PCBN Super-hard Tool Materials. *Diam Relat Mater* 16(3):435–445.
[7] Gekonde HO, Subramanian SV (2002) Tribology of Tool–chip Interface and Tool Wear Mechanisms. *Surface and Coatings Technology* 149(2):151–160.
[8] Hoier P, Malakizadi A, Klement U, Krajnik P (2019) Characterization of Abrasion- and Dissolution-induced Tool Wear in Machining. *Wear* 426-427:1548–1562.
[9] Gustafson P (1987) A Thermodynamic Evaluation of the C–Fe–W System. *Metallurgical Transactions A* 18(2):175–188.
[10] Sundman B, Ågren A (1981) A Regular Solution Model for Phases with Several Components and Sublattices, Suitable for Computer Applications. *Journal of Physics and Chemistry of Solids* 42(4):297–301.
[11] Naraghi R, Selleby M, Ågren J (2014) Thermodynamics of Stable and Metastable Structures in Fe–C System. *Calphad* 46:148–158.
[12] Kramer BM, Judd PK (1985) Computational Design of Wear Coatings, Journal of Vacuum Science &amp. *Technology A* 3(6):2439–2444.
[13] Pavlina EJ, Speer JG, Van Tyne CJ (2012) Equilibrium Solubility Products of Molybdenum Carbide and Tungsten Carbide in Iron. *Scripta Materialia* 66(5):243–246.
[14] Attia MH, Kops L (2004) A New Approach to Cutting Temperature Prediction Considering the Thermal Constriction Phenomenon in Multi-layer Coated Tools. *CIRP Annals* 53(1):47–52.
[15] Childs THC (2019) Revisiting Flow Stress Modelling for Simulating Chip Formation of Carbon and Low Alloy Steels. *Procedia CIRP* 82:26–31.
[16] Malakizadi A, Cedergren S, Sadik I, Nyborg L (2016) Inverse Identification of Flow Stress in Metal Cutting Process Using Response Surface Methodology. *Simulation Modelling Practice and Theory* 60:40–53.
[17] Shi B, Attia H (2009) Modeling the Thermal and Tribological Processes at the Tool-chip Interface in Machining. *Machining Science and Technology* 13(2):210–226.
[18] Saez-de-Buruaga M, Aristimuño P, Soler D, D'Eramo E, Roth A, Arrazola PJ (2019) Microstructure Based Flow Stress Model to Predict Machinability in Ferrite–pearlite Steels. *CIRP Annals* 68(1):49–52.

Please cite this article as: A. Malakizadi et al., Physics-based approach for predicting dissolution–diffusion tool wear in machining, CIRP Annals - Manufacturing Technology (2020), https://doi.org/10.1016/j.cirp.2020.04.040